

Wind Directions Retrieval from SAR Image Combining the Spatial and Spectral Domains: A Novel Approach Using a Modified Circle Median Filter

Chao Yang^{1,a}, Kaijun Ren², Dongxiang Zhang¹ and Weichen Ni¹,

¹National University of Defense Technology, College of Computer, Changsha 410073, China

²National University of Defense Technology, College of Meteorology and Oceanography, Changsha 410073, China

Abstract. Sea surface wind is of great importance for weather forecasts, oil spill monitoring, etc. The retrieval of wind speeds from synthetic aperture radar (SAR) images generally requires the knowledge of wind directions. There are two conventional methods of retrieving wind directions from SAR images, namely, two-dimensional fast Fourier transform (2D FFT) method in the spectral domain and local gradients (LG) method in the spatial domain. However, the spectral method just works fine on open oceans and large image areas, such as 20×20km and the spatial method is likely aligned with wind streak. In this paper, a new approach which combines the wind directions retrieved from 2D FFT and LG with a modified cycle median filter (CMF) is proposed for improving the accuracy of 2D FFT-retrieved wind directions. The proposed method is validated at different spatial resolutions, and the resolution of FFT-retrieved wind directions can be improved to 3km×3km.

1 Introduction

Synthetic aperture radar (SAR) has been one of the most efficient instruments to obtain sea surface wind (SSW) information at high spatial resolutions over large areas. In 1986, Gerling et al. [1] found that the linear structure in the SAR image is related with the wind direction (WD) and extracted the WD from SAR spectra. Besides, marine atmosphere boundary layer (MABL) rolls were also observed in SAR images as linear streaks which are consistent with WD [2]. From then on, researches have paid great attention on retrieving WD based on the wind streaks in the SAR images.

The main methods of WD retrieval from SAR images including the fast Fourier transforms (FFT) [3], wavelet transform (WT) [4], local gradients (LG) [5], and so on. In 1996, Vachon et al. extracted WD through spectral analysis by FFT. But FFT has a weakness for small image, e.g. 10km×10km [6]. In 2003, LG which extracts WD by acquisition of the orthogonal of the most frequent gradient direction was proposed by Koch et al. [7] LG overcomes the shortcoming of FFT and works better than FFT on the spatial sampling of 10km× 10km, even 1km × 1km. The WD from a SAR image by FFT or LG exist 180°ambiguity, which can be removed referencing to weather model output, Doppler shift or land shadows[7, 8].

When retrieving WDs from a SAR image, the SAR image is divided into a set of wind vector cells (WVCs). The direction at each WVC is extracted by FFT or LG. However, there are some isolated impulses in WDs

because of noise. The essence different of FFT and LG is that they represent information from frequency domain and spatial domain respectively. In this way, considering combining the two information is meaningful. The cycle median filter (CMF) technique is frequently used for the ambiguity removal in wind vector retrieval from scattermetter [9, 10]. CMF select a wind vector that is the closest vector to the true wind out of a set of ambiguous wind vectors at each WVC [9]. In this way, CMF can be used to improve the accuracy of FFT-retrieved WDs by combining LG-retrieved WDs from a SAR image.

In this study, we use a modified CMF to improve the accuracy of FFT-retrieved WDs from SAR images by combining LG-retrieved WDs that represent the directions from the spatial domain. In addition, the method is validated with different spatial resolutions using WD from National Data Buoy Center (NDBC).

The remainder of this paper is organized as follows. In section 2, the data used in this study are introduced. Section 3 describes the proposed method in detail. The performance of the method is validated in section 4. Conclusions are drawn in section 5

2 Data

Sentinel-1 interferometric mode (IW) mode Ground Range Detected (GRD) Vertical-Vertical (VV) polarized SAR images can be download from European Space Agency (ESA) Sentinels Scientific Data Hub with a nominal resolution of 20×22m and pixel spacing of 10m

^a Corresponding author: yangchao16@nudt.edu.cn

Table 1. Information of SAR Images in IW mode.

	Start Time	End Time	Center Lat (°N)	Center Lon (°E)
1	2017-05-18T14:16:04Z	2017-05-18T14:16:29Z	36.7694	-123.3518
2	2017-05-18T23:35:38Z	2017-05-18T23:36:03Z	24.5454	-82.5721

Table 2. Information of in suit NDBC buoy.

Station	Latitude (°N)	Longitude (°E)	Wind Direction (°)	Time
46012	37.363	-122.881	318	2017-05-18-14-20
plsf1	24.693	-82.773	97	2017-05-18-23-40

in range and azimuth, respectively. In this study, we concentrate on WDs retrieval from VV-polarized SAR image. Geometric calibrations are carried out by The Sentinel Application Platform 5.0 (SNAP 5.0) [11].

Two Sentinel-1 IW mode SAR images with wind streaks were used in our study. Their information is listed in Table 1. Associated with SAR images, the in situ National Oceanic and Atmospheric Administration (NOAA) National Data Buoy Center (NDBC) buoys are collected, which are listed in Table 2, including WD at the same time.

3 Method

For wind vector retrieval from scatterometer, a modified median filter is used to select a unique wind vector out of a set of ambiguous wind vectors at each WVC. In this study, we regard WDs extracted by FFT and LG as ambiguous WDs.

For a set of data A with length of N and circular data $x_i \in A, 1 \leq i \leq N$, the median y can be expressed as:

$$y = \operatorname{argmin}_{x \in A} \sum_{i=1}^N |x - x_i| \quad (1)$$

Based on (1), a median filter is implemented by constructing a fixed-length data window which passes over the data and a set of median data is acquired. For a set of data A with length of N , window length is setted as M . At step j , the data in the window is $D_j = \{x_d | j - h \leq d \leq j + h, h = M/2\}$. As in the following, the expression of (1) can be rewritten as:

$$y_i = \operatorname{argmin}_{x \in D_j} \sum_{m=i-h}^{i+h} |x - x_m| \quad (2)$$

In order to apply the median filter into SAR image, extending (2) for two-dimensional data is necessary:

$$y_{ij} = \operatorname{argmin}_{x \in D_{ij}} \sum_{m=i-h}^{i+h} \sum_{n=j-h}^{j+h} |x - x_{mn}| \quad (3)$$

where $D_{ij} = \{x_{pq} | i - h \leq p \leq i + h, j - h \leq q \leq j + h, h = M/2\}$ is the data in $M \times M$ window.

We consider a two-dimensional WDs $W_{ij} = \{x_{mn}^1, x_{mn}^2 | x_{mn} \in D_{ij}\}$, where each grid point (m, n) has two WD values, which are associated with WDs assigned by the FFT and LG algorithm. Let F_{ij}, L_{ij} be the set of FFT-retrieved WD and LG-retrieved WD at grid point (i, j) . Thus,

$$W_{ij} = F_{ij} \cup L_{ij} \quad \text{for all } i, j \quad (4)$$

Let F_{ij} be the initial WD filed at (i, j) grid. In this way, expression (3) can be written as:

$$y_{ij} = \operatorname{argmin}_{x \in F_{ij}} \sum_{m=i-h}^{i+h} \sum_{n=j-h}^{j+h} |x - x_{mn}| \quad (5)$$

At the center of the filter window, we can get a set of medians $\{y_{ij}\}$ of each window. The modified CMF can be written as:

$$z_{mn} = \operatorname{argmin}_{k=\{1,2\}} \sum_{m=i-h}^{i+h} \sum_{n=j-h}^{j+h} |y_{ij} - x_{mn}^k| \quad (6)$$

where $x_{mn}^k \in W_{ij}$, z_{mn} is the new data in $M \times M$ window.

For each window, the purpose is to select the WD that is closest to the median of the window at each grid point in W_{ij} . The z_{mn} is the value from W_{ij} , which is closest to y_{ij} . In this way, we get a new WD filed $Z_{ij}^* = \{z_{mn}\}$. The Z_{ij}^* is used to replace F_{ij} , and the filter selection process continues for each grid point (i, j) to create new Z_{ij}^* . The whole process is repeated to select a new Z_{ij}^* until $Z_{ij}^* = F_{ij}$. In addition, the WDs from LG or FFT have 180° ambiguity, it's essential to remove 180° ambiguity with

WD from NDBC for both FFT-retrieved and LG-retrieved direction firstly.

In the WDs retrieved by FFT, the isolated impulses often happen because of the noise. For the smoothness and continuity of wind field, it's useful to replace isolated impulses with median value directly, but it's a statistical-based method. Our method that uses WDs from LG to replace the error directions from FFT is more meaningful. Besides, it's effective to improve the resolution of FFT-retrieved WDs.

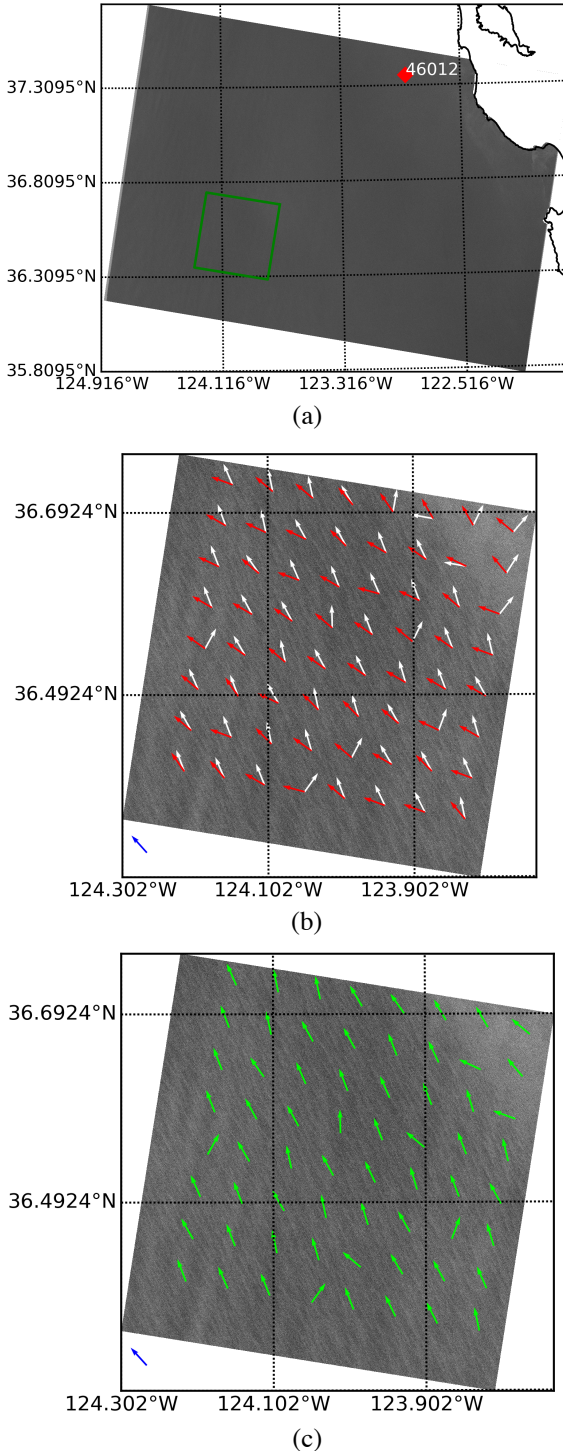


Figure 1. (a) The first SAR image listed in Table 1 in VV polarization with a resolution of 20m. (b) The WDs computed from 10m pixels on a 5km grid by FFT in white color and LG in

red color on a 44km by 44km sub-image that is indicated by green box in (a). (c) The WDs from our method on the same sub-image in (b). The blue arrow is the WD from buoy '46012' at the corresponding time.

4 Result

The wind streaks don't appear in all regions of the SAR image, so we find the wind streak patterns in a SAR image and apply FFT and LG to the sub-images at these locations. Besides, 180° ambiguity should be removed by buoy WD after applying FFT and LG. The default window size of our method is 5 and the step that the window passing the data is 2.

The first SAR image listed in Table 1 and acquired by Sentinel-1 IW mode in VV polarization with a resolution of 20m is shown in Figure 1(a). The SAR image is shown in grey and the land in the SAR image has been masked out. Besides, associated with the first SAR image, an in situ buoy is marked in red diamond in Figure 1(a). On a 44km by 44km sub-image that is indicated by green box in Figure 1(a), Figure 1(b) shows the WDs computed by FFT in white color and LG in red color. WDs are computed from 10m pixels on a 5km grid. The blue arrow (318°) in left-button is the WD from in situ buoy '416012'. The acquisition time of WD from buoy and SAR images is less than 5 minutes. In addition, the WDs here are in the same coordinate, in which the direction of the northward and eastward wind vector is 0° (or 360°) and 90° respectively.

As illustrated in Figure 1(b), the FFT-retrieved WDs is aligned with wind streaks closer than LG-retrieved WDs. That's the reason why we use LG-retrieved WDs to improving accuracy of FFT-retrieved WDs, rather than the other way around. However, there are some isolated impulses in FFT-retrieved WDs because of noise. Figure 1(c) is same as 1(b) except the green arrow that is the WDs from our method. It's obvious that our method revises FFT-retrieved WDs at right and top region. In general, FFT is effective on 20km×20km WVC and the difficulty of extracting WD by FFT is inversely related to the size of WVC [15]. When the wind resolution increases, FFT-retrieved WDs have more and more impulses. As shown in Figure 1, our method is effective on 5km×5km. In Figure 2a, the second SAR image listed in Table 1 and an in situ buoy marked in red diamond is shown. Figure 2(b) is a 37km×33km sub-image indicated by the green box in Figure 2(a). And the FFT-retrieved WDs in white color and WDs from our method in green color that are acquired on a 4km grid are illustrated in Figure 2b. In Figure 2b, the WDs from our method is almost covered by FFT-retrieved and the steps described in Section 3 just run once. Figure 2c is the same region as Figure 2b, but FFT-retrieved WDs and WDs from our method are both computed on a 3km grid. Note that, there are much more impulses in the FFT-retrieved WDs and we repeat twice the steps. In both 4km-grid and 3km-grid, our method shows a great performance.

In fact, CMF is always effective when over 50% of the FFT-retrieved WDs are right.however, wavelength of

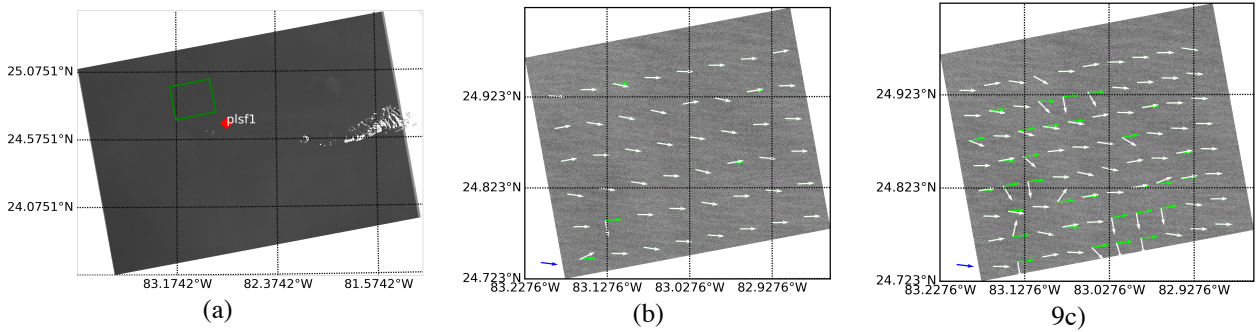


Figure 2. (a) The second SAR image listed in Tabell1 in VV polarization with a resolution of 20m. (b) The WDs computed from 10m pixels on a 4km grid by FFT in white color and our method in green color on a 37km by 33km sub-image that is indicated by green box in (a). (c) The WDs computed on a 3km grid by FFT in white color and our method in green color. The blue arrow is WD from buoy ‘plsf1’ at the corresponding time.

wind streaks is between 500m and 1500m [5]. When retrieving WDs from smaller regions, the wind information can't be acquired from speckle domain of SAR image. Therefore, it's more difficult to retrieve WD when the grids become smaller. In Figure 3, the FFT-retrieved WDs in white color are shown on a 1km grid and the results of our method in green color has changed the mostly wrong directions. However, impulses are too many to revise. Therefore, the effective of our method is limited by the weakness of FFT.

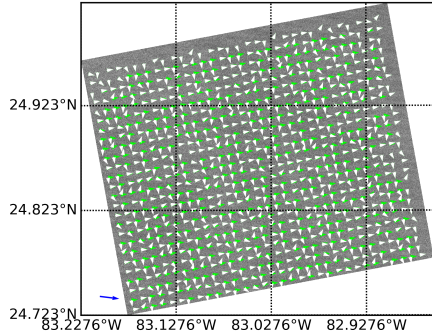


Figure 1. The FFT-retrieved WDs in white color and WDs from our method in green color on a 1km grid on the sub-image in Figure 2b.

5 Conclusion

In this paper, we concentrate on improving accuracy of FFT-retrieved WDs filed retrieved from SAR VV-polarized image by combining the FFT-retrieved directions and LG-retrieved directions. Considering the information of frequency domain and spatial domain, A modified CMF is proposed.

In this work, we modified CMF to select the WDs that is closest to the true WDs from FFT-retrieved WDs and LG-retrieved WDs. Two VV-polarized SAR image from Sentinel-1 IW mode are used to validate our method and the results show the effective. Besides, we analyse the performance of our method at different WDs resolutions. Since the wavelength of wind streaks is between 500m and 1500m, the resolution of FFT-retrieved WDs is limited. With the WDs resolution increases, it's more and

more difficult to retrieve WDs filed using our method, which is caused by the weakness of FFT. However, our method can get higher WDs resolution than that from FFT. Besides, according to our analysis, the new method has high performance in a 3km×3km gird.

In addition, the filter size and step length of our modified CMF are not discussed in this work, and we use filter size of 5 and set length of 2 as default. One thing that has to point out is that many WD retrieval methods can be used to replace LG in our method. The settings of CMF and the WD retrieval method in the spatial domain will be tuned in the future work.

Acknowledgement

This work was supported by the National Natural Science Foundation of China under Grant *****. The Sentinel-1 SAR data and the SNAP 5.0 software are available through the European Space Agency Sentinels Scientific Data Hub and European Space Agency Step Scientific Toolbox Exploitation Platform.

References

1. T W Gerling, *Journal of Geophysical Research: Oceans*, **91**, 2308(1986)
2. W Alpers, B Brümmer, *Journal of Geophysical Research: Oceans*, **99**, 12613–12621(1994)
3. P W Vachon, F W Dobson, *The Global Atmosphere and Ocean System*, **5**, 177–187(1996)
4. Yong Du, Paris W Vachon, *Canadian Journal of Remote Sensing*, **29**, 491–498(2003)
5. W Koch, *IEEE Transactions on Geoscience and Remote Sensing*, **42**, 702–710(2004)
6. Lizhang Zhou, Gang Zheng, Xiaofeng Li, Jingsong Yang, Lin Ren, Peng Chen, Huaguo Zhang, and Xiulin Lou, *Remote Sensing*, **9**(2017)
7. Biao Zhang, William Perrie, Jun A Zhang, Eric W Uhlhorn, and Yijun He, *Journal of Atmospheric and Oceanic Technology*, **31**, 272–286(2014)
8. J Horstmann, W Koch, *In Proceedings of IEEE Geoscience and Remote Sensing Symposium (IGARSS)*, 3102–3104(2003)

9. S J Shaffer, R S Dunbar, and S V Hsiao, *IEEE Transactions on Geoscience and Remote Sensing*, **29**, 167–174(1991)
10. B W Stiles, B D Pollard, and R S Dunbar, *IEEE Transactions on Geoscience and Remote Sensing*, **40**, 79–89(2002)
11. S F James, *Journal of Physics: Conference Series*, **926**, 012004(2017).